

An Association in the Aquila Star-Forming Region: High Resolution Infrared Spectroscopy of T Tauri Stars

E. L. RICE¹, L. PRATO², AND I. S. MCLEAN¹

ABSTRACT

We present the properties of a group of young stars associated with the well-studied T Tauri star system AS 353, located in the Aquila star-forming region. The association is identified using radial velocity measurements of sample objects selected from the Herbig and Bell Catalog based on their spatial proximity to AS 353. Radial velocities of nine objects were measured from multi-epoch high-resolution ($R \sim 30,000$) H -band spectra obtained with NIRSPEC on Keck II. High-resolution K -band spectra were also obtained for most of the sample objects. Spectral types and rotational velocities are determined for all objects in the sample. The multi-epoch H -band spectra were examined for radial velocity variations in order to detect possible spectroscopic binaries. Eight of the nine objects have radial velocities that are consistent within the $1-\sigma$ scatter of the sample. From their mean of -8 km s^{-1} these eight objects have a standard deviation of 2 km s^{-1} , which suggests that the sample stars are related. The ninth object shows significant radial velocity variations between epochs, characteristic of a spectroscopic binary. The overall multiplicity of the sample is high; we observed 13 stars in seven systems, identifying three new candidate binary components in this project. Many of the spectra reveal hydrogen emission lines typical of strong accretion processes, indicating that most of these objects harbor circumstellar disks and are less than a few million years old. Based on previous estimates, we adopt a distance of $200 \pm 30 \text{ pc}$ to the young stars in Aquila in order to calculate luminosities and place the stars on an H-R diagram. We discuss possible interpretations of the enigmatic pure emission line spectrum of HBC 684. This work represents the highest spectral resolution infrared observations to date of these intriguing, nearby young stars.

Subject headings: stars: T Tauri — stars: individual (AS 353A, AS 353B, HBC 294, HBC 681, HBC 682, HBC 683, HBC 684, FG Aql/G3) — open clusters

¹Department of Physics and Astronomy, UCLA, Los Angeles, CA 90095; erice@astro.ucla.edu

²Lowell Observatory, 1400 West Mars Hill Rd. Flagstaff, AZ 86001

and associations: individual (Aquila) — infrared: stars — techniques: spectroscopic — techniques: radial velocities

1. INTRODUCTION

Despite much study of the formation and evolution of young T Tauri stars, many questions remain concerning some of their most fundamental characteristics. Understanding the few million years of evolution between the protostellar and post T Tauri stages, including circumstellar disk accretion, planet formation, and disk dissipation, is crucial to understanding the formation of the Solar System and extra-solar planetary systems. One key approach to resolving these issues is striking a balance between in-depth studies of individual star-forming regions and observations of a variety of star-forming regions that differ in age, distance, stellar density, binary fraction, etc. The presence of T Tauri stars in a region indicates an age of 1–10 million years, the timescale for disk dissipation and the formation of gas giant planets around low mass stars (e.g., Zuckerman 2001). T Tauri stars are primarily identified by H α emission, IR and UV continuum excess, variability, and surrounding nebulosity (e.g., White & Ghez 2001; Zuckerman & Song 2004).

After 50 years of study, the young, low mass multiple star system AS 353, in the constellation Aquila, remains enigmatic. A \sim 5" pair, the system appears to be a mixed T Tauri binary, with the more massive component, AS 353A, showing signatures of a classical T Tauri star (cTTs), which is defined as having $\text{EW}(\text{H}\alpha) > 10 \text{ \AA}$ and excess infrared emission above the continuum level (Strom et al. 1989). The secondary, AS 353B, was classified as a weak-lined T Tauri star (wTTs, $\text{EW}(\text{H}\alpha) < 10 \text{ \AA}$), but has recently been resolved into a subarcsecond binary (Tokunaga et al. 2004). AS 353Ba was reclassified by Tokunaga et al. (2004) as a cTTs (but see §4.5.1 for further discussion). AS 353 is the exciting source of Herbig-Haro object HH 32, a highly collimated bipolar outflow (see Curiel et al. 1997, and references therein) and one of the only Herbig-Haro objects detected in 3.6 and 6 cm radio continuum (Anglada et al. 1992, 1998). Radio continuum emission has also been detected from the stars themselves, most recently attributed to the secondary rather than the primary (Avila et al. 2001).

The age of the AS 353 system was most recently determined by Prato et al. (2003) based on the location of AS 353B relative to the pre–main-sequence evolutionary tracks of Palla & Stahler (1999). This analysis resulted in an age of 5×10^5 years¹, or 1×10^6 years if

¹An error appears in Figure 7 of Prato et al. (2003) because of a missing minus sign in the $\text{Log} (L_*/L_\odot)$ for AS 353B. Data in the tables and text are accurate.

the binary nature of AS 353B is taken into account (see Appendix B of Prato et al. 2003). In this current paper we provide an updated discussion of the age of the AS 353 system as well as best estimates for the other objects in our sample (§4.2).

In addition to AS 353B, there are five T Tauri stars listed in the Herbig and Bell Catalog (1988, hereafter HBC) that are within $\sim 15^\circ$ of AS 353A, all between galactic latitudes of $b = -1^\circ$ to -6° . Their projected location in the crowded galactic plane complicates the study of these stars, as well as the search for additional young stars in the region. Few of the HBC Aquila objects have radial velocities or $vsini$ listed in the catalog, but from spectra with resolution lower than the observations presented here and/or using emission lines instead of absorption lines, with results that have uncertainties on the order of tens of km s^{-1} or more (Herbig 1977; Eislöffel et al. 1990; Fernández et al. 1995).

The original motivation for this project was to search for radial velocity variations in a sample of cTTs and wTTs in the vicinity of AS 353A as a means of identifying spectroscopic binaries. For double-lined spectroscopic binary systems, the relative velocity of each component, the mass ratio, and the center of velocity of the system can be determined. Obtaining dynamical masses of young stars is critical to the study of star formation because mass is the most fundamental of all stellar parameters, and evolutionary models that relate young star masses and ages with the observables L and T_{eff} are not yet calibrated. Furthermore, absolute radial velocities are important for determining if the young stars in the sample are actually related, i.e. if they were formed in the same molecular cloud. If they were, then it is expected that they have a low velocity dispersion relative to one another as well as with respect to the associated cloud (e.g., Herbig 1977).

High resolution infrared spectra, even a single echelle order, can reveal much more than radial velocities. In this study, what were assumed to be typical classical or weak-lined T Tauri stars were found to be surprisingly active systems with high rotational velocities, strong veiling, and unusual emission lines. Thus the goals of this project broadened to include the measurement of $vsini$, determination of spectral type, and characterization of the circumstellar environments of the targets, in addition to the radial velocity measurements. The sample is introduced in §2.1, and the NIRSPEC observations and their reduction are described in §§2.2 and 2.3, respectively. The data analysis, including line identification, determination of spectral type and $vsini$, and measurements of radial velocity variability and absolute radial velocity, are described in §3. The results are discussed in §4, including details of circumstellar environment, age, membership, and multiplicity. A summary appears in §5 along with suggestions for further studies of the Aquila star-forming region.

2. OBSERVATIONS & DATA REDUCTION

2.1. Sample

The targets were selected from the Third Catalog of Emission-Line Stars of the Orion Population (HBC) because of their spatial proximity to the well-studied T Tauri star AS 353A (HBC 292) and its companion, AS 353B (HBC 685). The names, coordinates, *H*-band magnitudes, and equivalent width of $\text{H}\alpha$ emission for each object are listed in Table 1. Coordinates are from SIMBAD² unless otherwise noted. The objects all lie within a region from 19h 00m to 19h 40m right ascension and -5° to $+11^\circ$ declination (Equinox 2000.0), placing them in the constellation Aquila. We adopt a distance of $200 \text{ pc} \pm 30 \text{ pc}$ (§4.2), which is consistent with both the most recent distance estimate to AS 353 ($150 \pm 50 \text{ pc}$, Prato et al. 2003) and to the dark cloud complex associated with HBC 294 ($230 \pm 30 \text{ pc}$, Kawamura et al. 2001). The physical size of this region on the plane of the sky is estimated to be $32 \pm 5 \text{ pc}$ by $58 \pm 9 \text{ pc}$ at this distance. Targets with previously determined spectral types range from early K to early M (Cohen & Kuhi 1979); several have been revised as a result of the work described in this paper.

As originally selected the sample consisted of six objects: HBC 292, 294, 681, 682, 683, and 684. During the course of the observations and subsequent analysis, the sample has grown to nine objects. HBC 682 was discovered to be a $1''$ visual binary upon the first observation with NIRSPEC. AS 353B was added to the sample in order to strengthen its association, using radial velocity measurements, with AS 353A. Because of its close proximity to HBC 681 and 682, a ninth star, FG Aql/G3 (Cohen & Kuhi 1979), was also observed.

2.2. Observations

Data were obtained with the cryogenic, cross-dispersed echelle spectrometer NIRSPEC installed on the Nasmyth platform of the Keck II telescope at the W.M. Keck Observatory on Mauna Kea, Hawaii (McLean et al. 1998, 2000). NIRSPEC employs a 1024×1024 ALADDIN InSb array detector operating at 30 K and sensitive to the range 0.95 to $5.4 \mu\text{m}$. All observations were taken in high-resolution mode with a slit size of $0.288'' \times 24''$ for non-AO observations and $0.027'' \times 2.26''$ for AO observations. The echelle mode and two pixel slit width provided a resolving power ($R = \lambda / \Delta\lambda$) of $R \sim 30,000$ for non-AO observations and $R \sim 35,000$ for observations behind AO, corresponding to a velocity resolution of $\sim 10 \text{ km s}^{-1}$

²SIMBAD is provided by the Centre de Données astronomiques de Strasbourg, France, <http://simbad.u-strasbg.fr/Simbad>.

per two-pixel resolution element in non-AO mode and ~ 8.6 km s $^{-1}$ in AO mode. Integration times ranged from two to five minutes per exposure for the Aquila objects. For each observation, a series of four spectra was taken in an ABBA pattern, nodding $\sim 10''$ along the slit between the A and B positions. Typical seeing was $0''.6$. Multiple ABBA sets were taken for fainter objects. Integration times ranged from 120 s to 300 s (Table 2).

H-band observations using the N5 filter (1.413 - 1.808 μm) were taken at several epochs between 2002 July and 2004 November to search for radial velocity variations. The intention was to observe each object a minimum of three times, however, it was possible to observe HBC 683 only twice and AS 353B and FG Aql/G3 only once. On 2004 May 27 and 28 (UT) the observations were made using NIRSPEC behind the Keck Adaptive Optics system (Wizinowich et al. 2000).

A *K*-band spectrum was obtained for each object on either 2003 September 07 (HBC numbers 294, 681, 682A&B, 683, and 684) or 2004 November 22 (AS 353A). AS 353B and FG Aql/G3 were not observed in *K*-band. Slightly different echelle angles resulted in different spectral coverage for the two sets of *K*-band observations. *K*-band spectra obtained on 2003 September 07 (not shown) suffered from poor subtraction of telluric absorption lines. Table 2 provides an observing log; instrument settings for all observations are summarized in Table 3.

2.3. Data Reduction

For data reduction we used the REDSPEC code,³ a package of IDL procedures created specifically for the reduction of NIRSPEC spectra by S. Kim, L. Prato, and I. McLean. Median-filtered dark and flat fields were created from multiple flat lamp and dark exposures for non-AO *H*-band observations. For AO observations and *K*-band observations, only a single flat and dark exposure were taken and differenced to create a final flat field. We determined the dispersion solution with a target star frame using OH night sky emission lines (Rousselot et al. 2000) or an arc lamp frame. The latter approach was necessary for the AO data because the night sky OH emission lines are too faint in the target frames. Based on the error analysis reported in Prato et al. (2002), we assign an uncertainty of 1 km s $^{-1}$ to the dispersion of each target.

We used *H*-band order 49 (1.545 - 1.567 μm) for the radial velocity measurements because of the presence of many narrow atomic and molecular absorption lines and the lack

³<http://www2.keck.hawaii.edu/inst/nirspec/redspec/>

of telluric absorption lines. Therefore, no division by a telluric A0 star was needed for order 49 spectra. In our K -band analysis we focused on the $\text{Br}\gamma$ line in order 35 (2.159 - 2.190 μm); orders 33, 36 and 37 were also reduced.

Reduction of order 35 was complicated by the presence of the broad $\text{Br}\gamma$ absorption in the telluric A0 star spectrum. To remove this intrinsic spectral feature while retaining the telluric features, we reduced the order 35 A0 star spectrum leaving the broad $\text{Br}\gamma$ and narrow terrestrial features intact. In a second reduction, we interpolated over the narrow telluric absorption lines only, leaving the $\text{Br}\gamma$ feature intact. The A0 star spectra resulting from these two reductions were then subtracted and the difference spectrum was renormalized to a continuum of 1.0, creating a spectrum of telluric features only. Target spectra were then divided by this corrected A0 star spectrum to remove the telluric lines.

The spectra were transformed onto a heliocentric reference frame and the continua were flattened and normalized to a value of 1.0. The signal to noise ratio (SNR) of the spectra was estimated by determining the maximum peak-to-peak variation in an order and dividing this by a factor of 4 to estimate the noise. The SNR appears in the last column of Table 2.

3. RESULTS AND ANALYSIS

3.1. High-Resolution Spectra

Figures 1 through 4 present the high-resolution spectra that will be discussed further in §4. Absorption and emission lines were identified using atlases of the solar spectrum and sunspot umbral spectrum in the near-infrared (Livingston & Wallace 1991; Wallace et al. 2001). K -band line identifications are from Table 4 of Prato et al. (2003). Individual objects are discussed in detail in §4.5.

Almost 40 absorption lines (some blended) were identified in the order 49 spectra of the object with the lowest rotational velocity, HBC 683, and therefore the sharpest lines. Fewer individual lines are identified in spectra with higher rotational velocity because nearby lines become increasingly blended as $vsini$ increases. The vast majority of the lines are atomic: mainly neutral Fe, some neutral Ti, Ni, and Si, and possibly S and C are identified. Intrinsic OH absorption appears in most spectra and a possible detection of CN emission in HBC 684. Significant H -band veiling in all of the absorption line object spectra is evident when these are compared to template spectra at similar $vsini$. Strong emission lines of very different nature were detected in order 49 for two objects: Br16 in AS 353A and multiple atomic, and possible molecular, lines in HBC 684.

In the K -band spectra for the sample, neutral atomic lines, such as Na, He, Al, and Mg, are observed in orders 33, 34, 36, and 37 (e.g., Figure 3). Br γ appears in order 35. Molecular lines of CO (orders 32 and 33) and H₂ (order 36) are also present.

The equivalent widths (EW) of the Br γ line ($n=7-4$, $\lambda=2.1661\text{ }\mu\text{m}$) were calculated for all objects observed in the K -band. For AS 353A, the Br γ EW, $-22\pm1\text{ }\text{\AA}$, is consistent with the Br γ EW of $-21\pm1\text{ }\text{\AA}$ from Prato et al. (2003), derived from low spectral resolution ($R\sim800$) observations made in 1996. EW was also calculated for the Br16 ($n=16-4$, $\lambda=1.5661\text{ }\mu\text{m}$) line observed in H -band order 49 of AS 353A. Line fluxes were calculated using the equivalent widths and K -band magnitude from *2MASS*. The uncertainty of the EW calculations is approximately $\pm1\text{ }\text{\AA}$, corresponding to an uncertainty of $\lesssim0.5\text{ W}\text{--}\text{m}^{-2}\times10^{-16}$ for the Br γ line fluxes and $\sim0.3\text{ W}\text{--}\text{m}^{-2}\times10^{-16}$ for the Br16 line fluxes. Brackett line EWs and fluxes appear in Table 4.

3.2. Spectral Types and $vsini$

The lines that were primarily used to determine spectral type were two Fe lines at $1.56259\text{ }\mu\text{m}$ and $1.56362\text{ }\mu\text{m}$ and a stellar OH doublet between them at $1.56314\text{ }\mu\text{m}$ in order 49. For a K1 star, the Fe lines are prominent and the OH line is nearly absent. For later K spectral types, the Fe lines monotonically weaken while the OH line strengthens; all three lines are of approximately equal strength for spectral type M1.

Bender et al. (2005) convolved rotation profiles from Gray (1992) with the spectra of observed spectral type standard stars, resulting in template spectra, for a range of spectral types, with $vsini=0, 2, 4, 6, 8, 10, 12, 15, 20, 25, 30, 40$, and 50 km s^{-1} . Examples of the template spectra with $vsini=10\text{ km s}^{-1}$ are presented in Figure 5; these objects are listed in Table 5. Uncertainties in the radial velocities of the template spectra are on the order of 1 km s^{-1} (Prato et al. 2002). The best fit spectral types were estimated by comparison with these standard star template spectra from Bender et al. (2005) and then confirmed with cross-correlation. The spectral types are accurate to at least two subclasses; there are templates for about every second subclass, but the difference between the template spectra is generally well-defined, especially in the Fe and OH lines mentioned above.

Because of veiling of the object spectra by continuum emission from reprocessing in circumstellar disks and accretion-induced excesses, cross-correlation yields an artificial best fit for high values of $vsini$. Therefore, the $vsini$ of each object was determined by visual inspection and comparison to rotated spectral templates alone. The spectral type and $vsini$ for each object in the sample appear in Table 6.

3.3. Radial Velocities

Radial velocities were measured by cross-correlating the target spectra with the best fit template spectrum from Bender et al. (2005). Spectra of HBC 684 were inverted because the typical absorption lines appear in emission for this object (see §4.5.5). Before cross-correlation, spectra were converted to the heliocentric reference frame, interpolated onto the same wavelength basis as the matching template spectrum, and rebinned by a factor of ten.

Because of the strong Br16 emission line in order 49, a different approach was used to measure the radial velocity of AS 353A. Absorption lines are more reliable for the measurement of radial velocity of an object because emission lines are produced by accretion flows or stellar winds, which have their own characteristic radial velocities. Therefore, we avoided the strong Br16 emission line in the spectra of AS 353A and used only the absorption lines shortward and longward of Br16 in the cross-correlation.

To estimate the uncertainties in the radial velocity measurements, the target spectra were cross-correlated with five template spectra of varying rotational velocity and spectral type, including the best-fit template. The standard deviation of the resulting radial velocity measurements was less than 2 km s^{-1} for all targets other than HBC 682A and HBC 684. For several targets the standard deviation of measurements was less than 1 km s^{-1} . We therefore adopt an uncertainty in the measurement of 2 km s^{-1} for all targets. This is consistent with the more formal uncertainties for the same method derived by Prato et al. (2002) and Mazeh et al. (2002).

We measured each object’s radial velocity at every epoch observed. Table 7 lists the objects in column (1), the UT dates of observation in column (2), and the radial velocities measured for each object at each epoch in column (3). For each object, we averaged the radial velocities over all epochs. These average values are reported in column (4) of Table 6. The standard deviation and the number of epochs for each target appear in columns (5) and (6) of Table 6. No average radial velocity is reported for HBC 682A because of the large variations between epochs. Standard deviations are not given for FG Aql/G3 and HBC 685 because only one observation of each object was made.

Targets were initially examined for radial velocity variability by cross-correlating spectra taken at different epochs. For all objects except HBC 682A, radial velocity variations were less than $\sim 4 \text{ km s}^{-1}$, with typical values around $1\text{--}2 \text{ km s}^{-1}$. This is within the estimated uncertainty of the radial velocity measurements. Radial velocity variations for HBC 682A were as large as 12 km s^{-1} . Velocity shifts between spectra from AO and non-AO observations were systematically higher than the typical velocity shifts between non-AO spectra from different epochs. This may be the result of the different approach to the dispersion solution

necessary with AO observations. The OH night sky lines used for the non-AO dispersion are distributed regularly throughout order 49, allowing for an excellent solution. The arc lamp lines required for the AO observations' dispersion solution are only four and their distribution across order 49 is sparse.

4. DISCUSSION

4.1. Circumstellar Properties

To determine the general circumstellar properties of the sample we plot $J - H$ versus $H - K$ colors from the *2MASS* photometry (Figure 6). Five of the objects have infrared excess according to this analysis, consistent with the same five objects that have $\text{EW}(\text{H}\alpha) > 10 \text{ \AA}$ (Table 1). Visual extinctions were estimated by dereddening the objects to the cTTs locus (Meyer et al. 1997) using

$$A_v = 13.83(J - H)_{obs} - 8.29(H - K)_{obs} - 7.43 \quad (1)$$

from Prato et al. (2003). The *2MASS* colors and the derived extinctions appear in Table 8. The average visual extinction of the sample is 1.6 magnitudes, not including AS 353A, which falls below the cTTs locus, possibly as the result of scattered light or a blue component to the color from continuum excess emission produced in accretion flows.

4.2. Age

To estimate the ages of the Aquila stars, we place all of the sample objects on an H-R diagram with the pre-main-sequence evolutionary tracks of Palla & Stahler (1999) (Figure 7). Luminosities were calculated using the method described in §3.3 of Prato et al. (2003). *2MASS* photometry was used for all objects except HBC 294, for which the angularly resolved photometry of Ageorges et al. (1994) was used. J -band bolometric corrections were from Hartigan et al. (Table 4 in 1994). Temperatures were taken from Luhman (2004) based on the spectral types listed in Table 6. Our adopted distance, 200 pc, was selected based on previous distance estimates to stars in this region. Prato et al. (2003) used 150 ± 50 pc as the distance to AS 353B, citing distance estimates to the Aquila Rift and Gould's Belt. Kawamura et al. (2001) estimated the distance to the dark cloud L694 to be 230 ± 30 pc based on star counts. We adopt a distance that is consistent with both of these estimates, 200 ± 30 pc. The bolometric luminosities for the components of HBC 682 have been corrected

for binarity based on their near-infrared flux ratio of 2.25 and 2.15, calculated from H - and K -band unpublished NIRC2 images, respectively. For AS 353B the flux ratio of the components is ~ 1 , and for HBC 682 the flux ratio was calculated in H - and K -band from unpublished NIRC2 images.

Based on a distance of 150 pc, the age of AS 353B was most recently determined to be 5×10^5 years (Prato et al. 2003). However, this calculation assumed that AS 353B was a single star; Tokunaga et al. (2004) has since identified the system as a close binary comprised of two M1.5 stars with a flux ratio of ~ 1 . In placing AS 353B on the HR diagram, we adopt our spectral type of M0 (Table 6 and §4.5.1), a distance of 200 pc, and one-half the luminosity determined from the unresolved system. Our resulting improved age for each component of AS 353B is ~ 1 Myr.

Although the vertical error bars are large because of the uncertain distances to the objects, the location of the ensemble on the H-R diagram suggests that most of the objects are approximately 1 Myr old. The large scatter in age could be attributed to the uncertainty in extinction down to the photospheres as well as uncertainty in the amount of infrared excess, both of which could lead to over- or under-estimation of bolometric luminosity for a particular object. Disk signatures in the young set of objects are consistent with an age of less than a few Myr. HBC 682A and B and especially FG Aql/G3 appear older, ~ 6 –12 Myr, consistent with their lack of emission lines and IR excesses, although the spectrum of FG Aql/G3 appears heavily veiled (Figure 1).

4.3. Membership of the Aquila Association

The standard deviation of the radial velocities of all the stars in the sample (~ 2 km s $^{-1}$), combined with many of the objects' signatures of youth and spatial proximity, are consistent with most if not all of the targets being members of a young stellar association. The average radial velocity for each object ranges from -6.8 to -11.4 km s $^{-1}$; all but two of the objects have radial velocities within one standard deviation of the mean of -8.6 km s $^{-1}$.

The only object for which a relatively constant radial velocity was not measured is HBC 682A, indicating that it may be a spectroscopic binary. Higher sampling frequency observations are needed to determine its mass ratio and center of mass velocity. However, we speculate that HBC 682A is a probable member of the Aquila association because of its proximity to HBC 682B ($\sim 1''$). Thus, it is likely that all nine stars in the sample belong to a single association that is part of the Aquila star-forming region.

4.4. Multiplicity

The multiplicity among the Aquila association members is comparable to that of Taurus, the well-studied star-forming region with the highest binary fraction (e.g. Simon et al. 1995; Simon 1997). Of seven systems that we observed, as many as thirteen components were found. Systems HBC 681 and HBC 682 were identified as multiple candidates for the first time. Two systems were known binaries (HBC 294 and HBC 682) and at least one is triple (AS 353). Additionally, HBC 682A may be a spectroscopic binary (§4.5.3) and HBC 681 may have a low-mass companion (§4.5.2).

4.5. Notes on Individual Objects

4.5.1. AS 353A & B (HBC 292 & HBC 685)

The order 49 spectra from the three observations of AS 353A are presented in Figure 2. AS 353A is best fit by a K5 template spectrum with $vsini=10$ km s $^{-1}$, somewhat later than the K2 spectral type previously reported in the literature (Tokunaga et al. 2004). The order 49 spectrum from the observation of AS 353B presented in Figure 1 is best fit by an M0 template spectrum with $vsini=20$ km s $^{-1}$, which is similar to the M1.5 spectral types found for both components of this subarcsecond binary by Tokunaga et al. (2004) using low resolution K -band spectra.

Strong Br16 ($n=16-4$) emission dominates the spectrum of AS 353A in order 49. A rise at the short wavelength end of the 2004 July 22 (UT) spectrum also suggests the presence of Br17, although the majority of the line falls outside the spectral coverage of the order. These strong Brackett lines are consistent with the strength of the H α detected in the optical (Herbig & Bell 1988) and confirmed by us in a visible light echelle spectrum (not shown). However, it is unusual to see what are presumably photospheric absorption lines superimposed on the emission line. The emission line appears to shift relative to the absorption lines between epochs. The veiling also appears variable; for example, the absorption lines are markedly deeper in the UT 2004 July 22 spectrum than in earlier spectra (Figure 2).

Selected orders of the K -band spectra of AS 353A along with probable feature identifications are presented in Figure 3. Order 35 shows strong Br γ emission, which is again consistent with the strong H α emission. Also apparent in the K -band spectra are atomic Mg, Al, and He, the CO(2–0) bandhead, and possibly H $_2$, all in emission. This rich emission spectrum is also apparent at low resolution ($R\sim760$) (Prato et al. 2003) and in the optical (Eislöffel et al. 1990).

Both AS 353A and B occupy unusual locations on the color-color diagram. The position of AS 353A indicates significant IR excess, consistent with the origin of the strong hydrogen emission in a circumstellar disk. The detection of AS 353 by the *IRAS* satellite (*IRAS* 19181+1056; the components are unresolved in the *IRAS* beam) also points to the presence of warm dust in the system (Weaver & Jones 1992). However, AS 353A lies *below* the cTTs locus, which may be the result of abundant scattered light in the circumstellar environment or a blue component of excess continuum emission from accretion flows. AS 353B does not show IR excess on the color-color diagram, which is consistent with its classification as a wTTs based on the strength of its H α emission. However, the extinction is larger than that of other cluster members if it is dereddened to the cTTs locus.

The prominent neutral hydrogen emission from AS 353A is likely a combination of accretion and stellar winds. H α emission is the primary characteristic used to identify circumstellar accretion (White & Ghez 2001). However, a strong stellar wind is indicated by other characteristics of this system, namely, that it is the exciting source of HH 32, a system of bright, compact emission line regions that are produced by a highly collimated bi-polar outflow (Curiel et al. 1997). The H α emission from AS 353A also displays a P Cygni profile with absorption in the blue wing of the emission line (Fernández et al. 1995), which indicates outflow from the star.

The similar radial velocity measurements of AS 353A and B (-11.4 and -10.7 km s $^{-1}$, respectively) and similar proper motions measured by Herbig & Jones (1983) make it likely that they are indeed a bound pair. Therefore, AS 353 is a mixed T Tauri system in which the more massive component is a cTTs while the secondary is a wTTs, which is thought to be more evolved than a cTTs. The slight infrared excess implied by the $K - L$ color of AS 353Ba by Tokunaga et al. (2004), 0.56 magnitudes, suggests the possible presence of circumstellar material around at least one of the AS 353B components. However, if the K - and L -band magnitudes for AS 353Ba are dereddened by an A_V of 2 magnitudes (Prato et al. 2003), the resultant $K - L$ color is 0.44 magnitudes. For an A_V of 3 magnitudes (this paper), the dereddened $K - L$ color is 0.37 magnitudes. Therefore, if circumstellar material is present at all around AS 353Ba, it is likely to be found at an advanced stage of dispersion. Possibly the binarity of AS 353B has played a role in the relatively early dissolution of its circumstellar disks.

It has been suggested that AS 353A is also a close binary (Tokunaga et al. 2004). If true, this would complicate the idea that binarity drives accelerated disk evolution, as AS 353A harbors one of the most substantial and active circumstellar disks known. Tokunaga et al. (2004) find no evidence for a companion object down to a separation of $0.1''$, corresponding to 20 AU for a distance of 200 pc to the system. If we assign AS 353A a mass of $1.2 M_\odot$

(Figure 7), the velocity signature induced by a companion object with a mass of $0.8 M_{\odot}$ in a circular orbit is about 7.5 km s^{-1} . Any higher mass companion would result in a larger amplitude of radial velocity variability in AS 353A, whereas any inclination of the system’s orbit out of the plane of our line of sight, a larger distance to the system than 200 pc, or a smaller mass companion, would result in smaller amplitude velocity variations. Over an interval of two years, however, no radial velocity variation greater than 1σ was measured between our three observations. Our observations, however, may be insensitive to highly eccentric spectroscopic binary orbits (e.g. Reipurth 2000).

4.5.2. HBC 294, HBC 681, & HBC 683

HBC 294 is best fit by a K7 template spectrum with $vsini=25 \text{ km s}^{-1}$. This agrees with the spectral type reported in the HBC. The radial velocity is well-determined, with a standard deviation of $< 0.5 \text{ km s}^{-1}$ based on measurements from three different epochs. HBC 294, also known as V536 Aql, is a typical cTTs, with $\text{Br}\gamma$ emission detected in our K -band observations and $\text{H}\alpha$, $\text{Pa}\beta$, and optical forbidden emission lines reported in the literature, indicative of accretion from a circumstellar disk. Whelan et al. (2004) describe evidence for a bipolar outflow from the system as well.

Ageorges et al. (1994) first discovered HBC 294 to be a binary with an $0''.52$ separation at a position angle of 17° . The unresolved near-IR excess observed in the system indicates warm dust surrounding at least one of the stars. The *IRAS* PSC flux measurements of HBC 294 (*IRAS* 19365+1023) reveal even greater mid- to far-IR fluxes than those of AS 353A at all but $100 \mu\text{m}$ (Weaver & Jones 1992). It is unclear whether the circumstellar material is located around one or both components of this binary. The lower $100 \mu\text{m}$ flux suggests that circumstellar material is truncated by the binary companion. The extinction required to deredden HBC 294 to the cTTs locus is comparable to the average extinction of the sample.

A K5 template with $vsini=20 \text{ km s}^{-1}$ provided the best fit to the spectrum of HBC 681. The $\text{H}\alpha$ emission of HBC 681, $\text{EW}=35 \text{ \AA}$, is relatively low for the cTTs in this sample, but still well above the 10 \AA cTTs limit. A clear IR excess is indicated by the location of HBC 681 on the color-color diagram. We identified a faint potential companion to HBC 681 at separation $\sim 1''.2$ and a position angle of $\sim 195^\circ$. The $H-K$ color of this object is $\sim 0.3-0.4$, typical of an unreddened M6 star, which, at the age of the Aquila association, would be substellar. However, the proper motion of this object must be observed to determine if the two objects are indeed related as HBC 681 is located in the direction of the galactic plane, and hence the field is crowded with faint background objects.

For the spectrum of HBC 683, we found a best fit using a K7 template spectrum with $v\sin i=15$ km s $^{-1}$. This is later than the spectral type of K1 reported in the HBC. The 2003 September 08 (UT) order 49 spectrum of HBC 683 is one of the best for line identification because of the high signal to noise ratio and low $v\sin i$ relative to the rest of the sample. HBC 683 is a typical cTTs and has the strongest H α and Br γ emission in our sample after AS 353A. HBC 683 also shows a clear IR excess in the color-color diagram (Figure 6). These properties are all consistent with its cTTs classification and the presence of an actively accreting circumstellar disk.

4.5.3. HBC 682 A & B

As a result of the observations presented in this paper, HBC 682 was discovered to be a visual binary with a separation of $\sim 1''$. HBC 682A is best fit by a K5 template spectrum with $v\sin i=50$ km s $^{-1}$, and HBC 682B by a K7 template spectrum with $v\sin i=30$ km s $^{-1}$. Both of these spectral types are earlier than that of M0 reported in the HBC.

Although the spectra of both components of HBC 682 have similar H - and K -band features, there are striking rotational and radial velocity differences between the two. HBC 682A has the broadest absorption lines in our sample, while HBC 682B is more typical. A consistent radial velocity was not measured for HBC 682A because of the large variations between epochs (Table 7). This may be in part because of the wide and shallow absorption lines that make precise measurement of radial velocity more difficult. However, the radial velocity variations measured in 5 different epochs, were significantly larger than the typical variation for other objects, e.g., 1–2 km s $^{-1}$. HBC 682A is therefore a candidate spectroscopic binary. We speculate that HBC 682A and B are bound because of their close proximity. Verification by component proper motion measurements and by determination of the center of mass velocity of the HBC 682A spectroscopic binary is needed, particularly in that this system is located in projection on to the galactic plane and hence confusion with background sources is possible.

The angularly unresolved HBC 682 system shows no IR excess, consistent with its weak H α and lack of Br γ emission. However, the classification of HBC 682 is complicated by the fact that it has only recently been resolved into a visual binary, and may in fact be a hierarchical triple. The components lack separate H α emission measurements and resolved near-IR photometry, both of which might provide additional information about their individual circumstellar environments.

4.5.4. FG Aql/G3

An M0 template with $vsini=15$ km s $^{-1}$ provided the best fit to the FG Aql/G3 system. The only observations of this object since Cohen & Kuhi (1979) are from *2MASS* and *DENIS* (Deep Near Infrared Survey), which combined provide *I*-, *J*-, *H*- and *K*-band photometry. No IR excess is detected. There are as yet no known signatures of youth associated with FG Aql/G3; Cohen & Kuhi (1979) did not detect H α emission from this star and we did not observe it in the *K*-band. The *H*-band spectrum, however, appears highly veiled. The location within 20" of three cluster members and FG Aql/G3's measured radial velocity are consistent with cluster membership. However, further evidence is needed to confirm the youth of this object.

4.5.5. HBC 684

The spectra from the three observations of HBC 684 are presented in Figure 4. The inverted order 49 spectrum of HBC 684 is best fit by a K5 template spectrum with $vsini=40$ km s $^{-1}$. The source of the emission lines in the spectra of this star is enigmatic. An examination of the FITS files revealed that the emission lines appeared in the raw data. Furthermore, emission lines were apparent in all orders of the raw *H*- and *K*-band data.

Although emission lines associated with accretion are common for young stars, they are usually manifested in strong hydrogen lines and only occasionally in other species, such as CO and neutral Na (Appenzeller & Wagner 1989; Eisloffel et al. 1990; Greene & Lada 1996; Prato et al. 2003). HBC 684 shows only modest H α (11 Å in the HBC and \sim 13 Å in our unpublished visible light spectrum) and Br γ emission, while most of the atomic lines in order 49, mainly Fe but possibly Ti, Si, and Ni as well, all appear in emission. We have tentatively identified lines of OH and CN also in emission; see Figure 4 and Table 10 for line identifications. In addition to these molecular lines in order 49, many emission lines probably arising from OH were identified in orders 46, 47, 48, and 50, and several emission lines from CN in orders 48 and 50. All of the typical cTTs in this sample (HBC 294, HBC 681, and HBC 683) show stronger H α emission, and all but HBC 294 show stronger Br γ emission as well (Table 4).

Greene & Lada (1996) reported a rich near-IR emission line spectrum of the class I young stellar object *IRAS* 04239+2436 in Taurus. Although the resolution was modest ($R\sim 500$), over a dozen emission features were identified in the observed spectral range of 1.1 to 2.5 μ m. Probable features included several CO bandheads, Br γ , Br10, Br11, Br13, Br14, Pa β , H₂, and neutral He. Only the neutral Ca triplet at $\lambda=2.26$ μ m was observed in

absorption. We know of no other spectra, however, with low-excitation atomic and possibly molecular species in emission as they appear in HBC 684’s *H*-band spectra.

The Palomar Observatory Sky Survey and *2MASS* images show some nebulosity to the north and east of HBC 684; however, this diffuse emission was not evident in more recent *H*-band images (in short, 0.1s exposures) taken with the NIRSPEC Slit-viewing Camera (SCAM) in 2004 November. HBC 684 is an *IRAS* source (*IRAS* 19046+0508) with PSC fluxes at 12, 25, 60 and 100 μm even greater than those of AS 353A, which indicates a considerable amount of warm dust around the star. The near-IR excess of HBC 684 is the strongest in our sample (Figure 6).

We suggest four mechanisms that might produce spectra such as those observed in HBC 684. First, accretion could be creating an oblique shock close to the photosphere of the star, which occurs when the accretion speed equals the escape velocity of the star. However, the lack of strong H α emission limits the amount of circumstellar material that could be accreting from a circumstellar disk. Furthermore, our H α spectrum shows a clear P Cygni profile, characteristic of outflow, but not infall.

HBC 684’s emission lines could also be produced by an inversion layer resembling the chromosphere of the Sun. If some blocking mechanism such as a circumstellar disk, similar to the function of the Moon during total solar eclipse, could be construed, a phenomenon resembling a solar flash spectra might be produced (see Herbig 1990). Stellar chromospheres are heated by stellar coronae; the X-ray emission frequently observed in young stars is thought to originate in the corona (Neuhauser et al. 1995, e.g.). However, the nearest known X-ray source in the vicinity of HBC 684, 1RXS J190722.4+051231 in the *ROSAT* All-Sky Survey Faint Source Catalog,⁴ is 3.2’ away and is therefore probably not associated with HBC 684.

A transient impact on the photosphere could provide sufficient energy to excite the atomic metals that are observed in emission. In 1994 July fragments of the comet Shoemaker-Levy 9 plunged into the atmosphere of Jupiter. Costa et al. (1997) observed the plume of the most energetic impact and found atomic emission lines from neutral Na, Fe, Ca, Li in the optical spectrum. Infrared spectra of another impact show molecular band/line emission, including CH₄ and CO(2–0) (Knacke et al. 1997). Given the few million year age of this association and the evidence for circumstellar material around HBC 684, it is plausible that

⁴The *ROSAT* All-Sky Survey Faint Source Catalog is queried via the High Energy Astrophysics Science Archive Research Center(HEASARC) Browse Main Interface. HEASARC is a service of the Laboratory for High Energy Astrophysics at NASA/GSFC and the High Energy Astrophysics Division of the Smithsonian Astrophysical Observatory.

planetessimals are forming around and may occasionally fall into the star. Indeed, the planet plunging phenomenon proposed to account for the high metallicity observed in extra-solar planetary systems (Armitage & Bonnell 2002) may be invoked in this case. The slow motion merger of a giant planet or brown dwarf could create the requisite energy for the Fe I emission lines (on the order of 6–7 eV) without exciting significant hydrogen emission. Such a merger would require a substantial circumstellar disk in order to abet angular momentum transfer; the presence of a disk is supported by the strong near- and mid-IR excesses observed in this system. The P Cygni profile in the H α emission line implies an outflow of 200 km s $^{-1}$. A planet plunging event might stimulate the velocity of such a jet. The duration of the effects of a merger is not known; we have observed consistent emission line spectra of HBC 684 on three separate occasions over a 14 month period. In 1981, a broad, strong P Cygni profile was already present (notes in HBC).

A final possibility we consider is the stimulation of line emission by fluorescence. We found that the upper energy level terms for the order 49 Fe I lines represent too broad a range of states for the production of all the *H*-band lines to be consistent with fluorescence originating in one particular pumping line. Furthermore, all the lines expected in a normal K5 star are present in the infrared spectra of HBC 684, except in emission. Compare this, for example, to HBC 682B, which has a similar spectral type and value of $v\sin i$. HBC 684’s emission lines also display similar line ratios as the corresponding absorption lines in a template spectrum or in HBC 682B. Some of the unusual features in the HBC 684 spectra may be the result of fluorescence, but we are skeptical that this is the explanation for the entire set of emission lines observed.

5. CONCLUSION

This paper presents the results of multi-epoch observations of a sample of nine young, late-type stars in the Aquila star-forming region. Sample objects were selected from Herbig & Bell (1988) based on their proximity to AS 353A and classification as a wTTs or cTTs. The high-resolution ($R \sim 30,000$) *H*-and *K*-band observations were made between 2002 July and 2004 November with NIRSPEC on Keck II. The initial goal of this project was to examine one *H*-band order of the multiple-epoch spectra for radial velocity variations in order to detect spectroscopic binaries. One radial velocity variable object was discovered and absolute radial velocities were measured for the remaining eight objects. Circumstellar properties of the stars were also examined via high-resolution *K*-band spectra and 2MASS photometry.

Eight of the nine sample objects appear to be members of the same association because

of similar radial velocities. The spatial extent of the known members, using our adopted distance of 200 ± 30 pc, is 32 ± 5 pc by 58 ± 9 pc. The ages of the observed objects exhibit a large scatter, with the youngest, most active members all of age $\sim 1\text{--}2$ Myr. Two systems appear to have ages between 6 and 12 Myr, and the oldest of these (FG Aql/G3) has not been confirmed to show signatures of youth. Therefore, the Aquila association of stars is apparently one of the youngest nearby star-forming regions. The visual extinction to the association is estimated to be about 1–2 magnitudes.

The circumstellar environments of associations members are varied, ranging from extremely active (AS 353A, whose winds drive HH 32) to nearly devoid of circumstellar material (AS 353B, HBC 682, and FG Aql/G3, which all lack IR excess and strong H α emission), with several typical cTTs in between (HBC 294, HBC 681, and HBC 683). The source of the atomic and molecular emission lines in the spectra of HBC 684 is as yet unknown, but may be caused by an inversion layer, increased accretion, fluorescence, or a transient impact. For the seven systems in this study, HBC 681, HBC 682, HBC 683, HBC 684, HBC 294, FG Aql/G3, and AS 353, there is a high total number of stars, thirteen at least, yielding ~ 2 stars per system. This multiplicity is significantly higher than even that of the Taurus region (~ 1.6 stars per system; Simon et al. 1995), although it applies to only a small sample and may be significantly impacted by observational biases. The extremely interesting stars identified to date in this association certainly warrant further investigation.

Much work remains to characterize this unusual star-forming region. The most pressing task is to confirm the existence of a larger association by searching for other young stars in the region and identifying radial velocities and proper motions of the new members. Obtaining a more accurate distance determination to the association will also be critical to unraveling the age-distance discrepancy. For the non-thermal radio source AS 353B, this could be accomplished with VLBI (e.g. Loinard et al. 2005). Once more complete membership is determined, the Aquila star-forming region can be characterized in terms of mass function, multiplicity fraction, and other parameters. Further observations in the millimeter, sub-millimeter, infrared, radio, and X-ray will also provide valuable information about the circumstellar environments of these objects, which will improve our understanding of key phases of pre-main-sequence stellar evolution.

6. ACKNOWLEDGMENTS

We thank the expert observing assistants and staff of the Keck Observatory for their capable help. Insightful discussions with C. McCabe, D. Hunter, M. Simon, S. Kenyon, E. Becklin, M. Jura, B. Zuckerman, S. Strom, G. Herbig, and B. Reipurth improved the

presentation of this paper. We are grateful to S. Zoonematkermani for providing some of the IDL procedures used in the analysis, to C. McCabe and G. Duchêne for obtaining several spectra for us in 2004 May, to M. Huerta for speedy reduction of the AS 353A and HBC 684 H α spectra taken at McDonald Observatory in 2005 November, and to Q. Konopacky for several NIRC2 images. We thank the anonymous referee for helpful comments. L. Prato was supported in part by NSF grant AST 04-44017. Data presented herein were obtained at the W. M. Keck Observatory, which is operated as a scientific partnership among the California Institute of Technology, the Universities of California, and the National Aeronautics and Space Administration. The observatory was made possible by the generous financial support of the W. M. Keck Foundation. The authors wish to recognize and acknowledge the very significant cultural role and reverence that the summit of Mauna Kea has always had within the indigenous Hawaiian community. We are most fortunate to have the opportunity to conduct observations from this mountain. This work made use of the SIMBAD reference database, the VizieR Service, the NIST Atomic Spectra Database, the NASA Astrophysics Data System, and the NASA/IPAC Infrared Service Archive.

REFERENCES

Ageorges, N., Ménard, F., Monin, J.-L., & Eckart, A. 1994, A&A, 283, L5

Anglada, G., Rodríguez, L. F., Cantó, J. Estalella, R., & Torrelles, J.M. 1992, ApJ, 395, 494

Anglada, G., Villuendas, E., Estalella, R., Beltrán, M. T., Rodríguez, Torrelles, J.M., & Curiel, S. 1998, AJ, 116, 2953

Appenzeller, I. & Wagner, S. 1989, A&A, 225, 432

Armitage, P. J. & Bonnell, I. A. 2002, MNRAS, 330, L11

Avila, R., Rodríguez, L. F., & Curiel, S. 2001, Rev. Mexicana Astron. Astrofis., 37, 201

Bender, C., Simon, M., Prato, L., Mazeh, T., & Zucker, S. 2005, AJ, 129, 402

Carpenter, J. M. 2001, AJ, 121, 2851

Cohen, M. & Kuhi, L. V. 1979, ApJS, 41 743

Costa, R. D. D., de Freitas Pacheco, J. A., Singh, P. D., de Almeida, A. A., & Codina-Landaberry, S. J. 1997, ApJ, 485, 380

Curiel, S., Raga, A., Raymond, J., Noriega-Crespo, A., & Canto, J. 1997, AJ, 114 2736

Eislöffel J., Solf, J., & Böhm, K. H. 1990, A&A, 237 369

Fernández, M., Ortiz, E., Eiroa, C., & Miranda, L. F. 1995, A&AS, 114 439

Gray, D. F. 1992, The Observation and Analysis of Stellar Photospheres (Cambridge: Cambridge University Press), 368

Greene, T. P. & Lada, C. J. 1996, ApJ, 461, 345

Hartigan, P., Strom, K. M., & Strom, S. E. 1994, ApJ, 427, 961

Herbig, G. H. 1977, ApJ, 214, 747

Herbig, G. H. 1990, ApJ, 360, 639

Herbig, G. H., & Bell, K. R. 1988, Lick Observatory Bull. 1111

Herbig, G. H. & Jones, B. F. 1983, AJ, 88 1040

Kawamura, A., Kun, M., Onishi, T., Vavrek, R., Domsa, I., Mizuno, A., & Fukui, Y. 2001, PASJ, 53, 1097

Knacke, R. F., Fajardo-Acosta, S. B., Geballe, T. R., & Noll, K. S. 1997, Icarus, 125, 340

Levrault, R. M. 1988, ApJ, 330, 897

Livingston, W. & Wallace, L. 1991, National Solar Observatory Technical Report 91-001

Loinard, L., Mioduszewski, A. J., Rodríguez, L. F., González, R. A., Rodríguez, M. I.. & Torres, R. M. 2005, ApJ, 619, 179

Luhman, K. L. 2004, ApJ, 617, 1216

Mazeh, T., Prato, L., Simon, M., Goldberg, E., Norman, D., & Zucker, S. 2002, 564, 1007

McLean, I. S., Becklin, E. E., Bendiksen, O., Brims, G., Canfield, J., Figer, D. F., Graham, J. R., Hare, J., Lacayanga, F., Larkin, J. E., Larson, S. B., Levenson, N., Magnone, N., Teplitz, H., & Wong, W. 1998, Proc. SPIE, 3354, 566

McLean, I. S., Graham, J. R., Becklin, E. E., Figer, D. F., Larkin, J. E., Levenson, N. A., & Teplitz, H. I. 2000, Proc. SPIE, 4008, 1048

Meyer, M. R., Calvet, N., & Hillenbrand, L. A. 1997, AJ, 114, 288

Neuhäuser, R., Sterzik, M.F., Schmitt, J. H. M. M., Wichmann, R., & Krautter, J. 1995. A&A, 297, 391

Palla, F., & Stahler, S. W. 1999, *ApJ*, 525, 722

Prato, L., Simon, M., Mazeh, T., McLean, I. S., Norman, D., & Zucker, S. 2002, *ApJ*, 569, 863

Prato, L., Greene, T. P., & Simon, M. 2003, *ApJ*, 584, 853

Reipurth, B. 2000, *AJ*, 120, 3177

Rousselot, P., Lidman, C., Cuby, J.-G., & Monnet G. 2000, *A&A*, 354, 1134

Simon, M., Ghez, A. M., Leinert, Ch., Cassar, L., Chen, W. P., Howell, R. R., Jameson, R. F., Matthews, K., Neugebauer, G., & Richichi, A. 1995, *ApJ*, 443, 625S

Simon, M. 1997, *ApJ*, 482, L81

Strom, K. M., Strom, S. E., Edwards, S., Cabrit, S., & Skrutskie, M. F. 1989, *AJ*, 97, 1451

Tokunaga, A. T., Reipurth, B., Gässler, W., Hayano, Y., Hayashi, M., Iye, M., Kanzawa, T., Kobayashi, N., Kamata, Y., Minowa, Y., Nedachi, K., Oya, S., Pyo, T., Saint-Jacques, D., Terada, H., Takami, H., & Takato, N. 2004, *AJ*, 127, 444

Wallace, L., Hinkle, K., & Livingston, W. C. 2001, National Solar Observatory Technical Report 01-001

Weaver, W. B. Jones, G. 1992, *ApJS*, 78, 239

Whelan, E. T., Ray, T. P., & Davis, C. J. 2004, *A&A*, 417, 247

White, R. J. & Ghez, A. M. 2001, *ApJ*, 556, 265

Wizinowich, P., Acton, D. S., Shelton, C., Stomski, P., Gathright, J., Ho, K., Lupton, W., Tsubota, K., Lai, O., Max, C., Brase, J., An, J., Avicola, K., Olivier, S., Gavel, D., Macintosh, B., Ghez, A., & Larkin, J. 2000, *PASP*, 112, 315

Zuckerman, B. 2001, *ARA&A*, 39, 549

Zuckerman, B. & Song, I. 2004, *ARA&A*, 42, 685

Table 1. THE SAMPLE

Primary Name	Other Name	R.A. ^a (J2000.0)	Dec. ^a (J2000.0)	<i>l</i> , <i>b</i> ^a (°, °)	<i>H</i> -band magnitude ^a	EW(H α) ^b (Å)
HBC 681	FG Aql/G1	19 02 22.20	−05 36 20.4	29.17, −4.98	9.429	35
FG Aql/G3	<i>2MASS</i> 190222.6−053522	19 02 22.60	−05 36 22.1	29.17, −4.98	12.019	...
HBC 682 ^c	FG Aql/G2	19 02 22.84	−05 36 15.8	29.18, −4.98	9.492	2.3
HBC 683	FH Aql	19 02 23.22	−05 36 37.3	29.17, −4.98	10.380	105
HBC 684 ^d	<i>IRAS</i> 19046+0508	19 07 09.87	+05 13 10.8	39.37, −1.11	8.555	11
AS 353A	HBC 292	19 20 30.99	+11 01 54.7	46.05, −1.33	9.161	150
AS 353B ^e	HBC 685	19 20 31.04	+11 01 49.1	46.05, −1.33	9.154	4.4
HBC 294 ^f	V536 Aql	19 38 57.41	+10 30 16.1	47.75, −5.57	8.102	52

^aR.A. and Dec. from *2MASS*; Galactic coordinates from SIMBAD

^bFrom Herbig & Bell (1988)

^c1" visual binary

^dSome confusion exists in the literature because of the identification of HBC 684 as WL 22 in several papers, including Herbig & Bell (1988), Levreault (1988), and Weaver & Jones (1992). In the SIMBAD database, WL 22 refers to a T Tauri star in Ophiucus.

^e0.24 binary

^f0.52 binary

Table 2. OBSERVING LOG

Date (UT)	Object	Filter	Integration Time (s)	Airmass	SNR
2002 July 18	AS 353A	N5	300	1.03	170
	AS 353B	N5	300	1.04	200
2003 August 10	HBC 681	N5	300	1.11	350
	FG Aql/G3	N5	220	1.11	250
	HBC 682 (A & B)	N5	180	1.11	280
2003 September 07	HBC 681	K	240	1.12	150
	HBC 682 (A & B)	K	200	1.13	180
	HBC 683	K	240	1.16	170
	HBC 684	K	120	1.11	170
	HBC 294	K	120	1.05	180
2003 September 08	HBC 681	N5	240	1.13	250
	HBC 682 (A & B)	N5	240	1.19	270
	HBC 683	N5	220	1.40	250
	HBC 684	N5	300	1.49	280
	HBC 294	N5	300	1.40	420
2004 May 27 (AO)	HBC 681	N5	300	1.25	210
	AS 353A	N5	300	1.02	170
2004 May 28 (AO)	HBC 682A	N5	300	1.22	250
2004 July 22	HBC 682A	N5	240	1.28	300
	HBC 681	N5	180	1.36	300
	HBC 684	N5	180	1.30	340
	AS 353A	N5	300	1.05	210
	HBC 294	N5	120	1.06	320
2004 November 21	HBC 683	N5	240	1.56	80
	HBC 684	N5	180	1.53	330
	HBC 294	N5	120	1.39	270
2004 November 22	HBC 682 (A & B)	N5	180	1.57	210
	AS 353A	K	240	1.49	340

Table 3. NIRSPEC INSTRUMENT SETTINGS

Filter	Date (UT)	Echelle Angle (°)	Cross-dispersion Angle (°)	Slit Size (Arcseconds)	Spectral Resolution
N5	2002 Jul. - 2004 Nov.	63.04	36.30	0.288 × 24	30,800 ^a
N5 (AO)	2004 May 27 & 28	63.04	36.30	0.027 × 2.26	35,900 ^b
K	2003 September 07	62.15	35.59	0.288 × 24	24,500 ^c
K	2004 November 22	62.84	35.59	0.288 × 24	29,000 ^c

^aOrder 49; calculated using the FWHM of an OH night sky line and averaged over all frames.

^bOrder 49; calculated using the FWHM of an arc lamp line and averaged over both nights.

^cOrder 35; calculated using the FWHM of an OH night sky line and averaged over all frames.

Table 4. MEASURED BRACKETT STRENGTHS

Object	Obs. Date	EW ^a (Å)	Line Flux ^b (W-m ⁻² × 10 ⁻¹⁶)
Br γ			
HBC 681	2003 September 07	-5	0.6±0.1
HBC 682A	2003 September 07	1	... ^d
HBC 682B	2003 September 07	1	... ^d
HBC 683	2003 September 07	-5	0.3±0.1
HBC 684	2003 September 07	-3	1.4±0.5
HBC 294	2003 September 07	0 ^c	0.2±0.4
AS 353A	2004 November 22	-22	3.8±0.2
Br16			
AS 353A	2002 July 18	-5	1.6±0.3
AS 353A	2004 May 27	-7	2.2±0.3
AS 353A	2004 July 22	-4	1.4±0.3

^aBr γ or Br 16 equivalent widths. Negative values indicate emission and positive values absorption. Uncertainties are ~ 1 Å.

^bFlux integrated over emission feature and corrected for continuum emission.

^cBr γ emission was observed in the spectrum of HBC 294, but the measured value was less than 0.5 Å.

^d Line flux was not calculated for absorption lines.

Table 5. SPECTRAL TYPE AND $vsini$ TEMPLATES^a

Object	Spectral Type
GL 275.2A	K1
HD 283750	K2
BS 8085	K5
BS 8086	K7
GL 763	M0
GL 752A	M2

^aTemplate spectra obtained from C. Bender, private communication.

Table 6. SPECTRAL TYPE, $vsini$, AND RADIAL VELOCITY

Object (1)	Spectral Type (2)	$vsini$ (km s ⁻¹) (3)	Radial Velocity (km s ⁻¹) (4)	Standard Deviation (km s ⁻¹) (5)	No. Spectra ^a (6)
HBC 681	K5	20	−7.4	0.9	4
FG Aql/G3	M0	15	−8.9	... ^b	1
HBC 682A	K5	50	... ^c	5.6	5
HBC 682B	K7	30	−6.8	1.5	3
HBC 683	K7	15	−6.8	0.8	2
HBC 684	K5	40	−7.2	2.2	3
AS 353A	K5	10	−11.4	1.1	3
AS 353B	M0	20	−10.7	... ^b	1
HBC 294	K7	25	−9.8	0.3	3

^aNumber of spectra used in radial velocity analysis.

^bOnly one observation.

^cSignificant variations in radial velocity between epochs – see Table 7.

Table 7. RADIAL VELOCITY MEASUREMENTS

Object	Obs. Date (UT)	Radial Velocity (km s ⁻¹)
HBC 681	2003 August 10	-8.1
	2003 September 08	-7.7
	2004 May 27	-6.4
	2004 July 22	-7.6
FG Aql/G3	2003 August 10	-9.4
HBC 682A	2003 August 10	-3.0
	2003 September 08	-13.2
	2004 May 28	-6.9
	2004 July 22	-6.8
	2004 November 22	-2.1
HBC 682B	2003 August 10	-5.9
	2003 September 08	-5.5
	2003 November 22	-8.5
HBC 683	2003 September 08	-7.4
	2004 November 21	-6.2
HBC 684	2003 September 08	-5.5
	2004 July 22	-7.2
	2004 November 21	-9.8
AS 353A	2002 July 18	-12.1
	2004 May 27	-10.1
	2004 July 22	-12.1
AS 353B	2002 July 18	-10.7
HBC 294	2003 September 08	-9.4
	2004 July 22	-9.8
	2004 November 21	-9.8

Table 8. COLORS AND EXTINCTION

Object	$J - H^a$	$H - K^a$	Visual Extinction ^b (mag)
HBC 681	0.925	0.636	0.1
FG Aql/G3	0.858	0.212	2.7
HBC 682	0.752	0.161	1.6
HBC 683	1.015	0.712	0.7
HBC 684	1.342	1.156	1.6
AS 353A	0.733	0.723	−3.3
AS 353B	1.029	0.396	3.5
HBC 294	1.042	0.706	1.1

^aColors calculated from *2MASS* photometry.

^bExtinction calculated using Equation 2, §5.3.

Table 9. MULTIPLICITY

Object	Multiplicity	Separation ($''$)	Position Angle ($^{\circ}$)
HBC 681	Possible low-mass companion	~1.2	~195
FG Aql/G3	Single
HBC 682	Binary, probable triple	~1	~160
A	possible SB
HBC 683	Single
HBC 684	Single
AS 353	Triple	5.6	174
B	Binary	0.24	107
HBC 294	Binary	0.52	17

Table 10. IDENTIFIED ABSORPTION LINES

Wavelength (μm)	Species	Label
1.54562	Fe	0
1.54635	Fe	1
1.54740	S	2
1.54797	Fe/S ^a	3
1.54829	S/Fe ^a	4
1.54897	Fe	5
1.54951	Fe	6
1.55009	Fe	7
1.55036	Fe	8
1.55053	Fe ^a	9
1.55103	C	10
1.55185	Fe	11
1.55236	Fe	12
1.55360	Fe	13
1.55385	Fe	14
1.55448	Ni	15
1.55463	Fe	16
1.55480	Ti	17
1.55552	Fe ^a	18
1.55596	Ni	19
1.55620	Si	20
1.55650	Fe	21
1.55710	Fe	22
1.55760	Fe	23
1.55833	Fe	24
1.55925	Fe	25
1.55958	Fe	26
1.56071	Ti	27
1.56085	Fe	28
1.56099	Ni	29
1.56154	Fe	30

Table 10—Continued

Wavelength (μm)	Species	Label
1.56179	Fe	31
1.56259	Fe	32
1.56314	OH	33
1.56336	Fe ^a	34
1.56362	Fe	35
1.56528	Fe	36
1.56571	Fe	37
1.56663	Fe	38
1.56695	Fe	39

Note. — Lines were identified using Livingston & Wallace (1991) and Wallace et al. (2001).

^aBlended

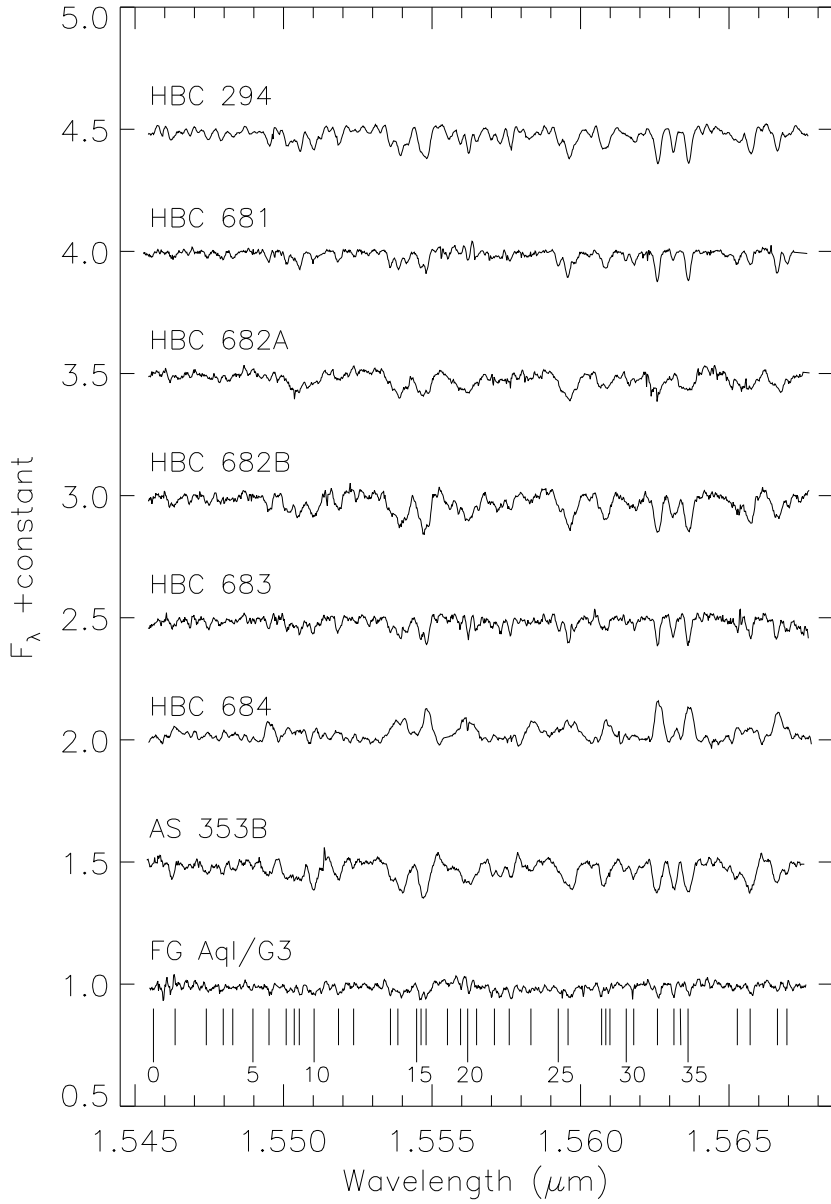


Fig. 1.— NIRSPEC order 49 spectra of eight sample objects. All spectra are from observations made on 2003 September 08 (UT) except for AS 353B (2002 July 18) and FG Aql/G3 (2003 August 10). Wavelength and species of identified lines are given in Table 10. All spectra have been wavelength-corrected for heliocentric and radial velocity, normalized to a continuum level of unity, and offset by 0.5 in flux.

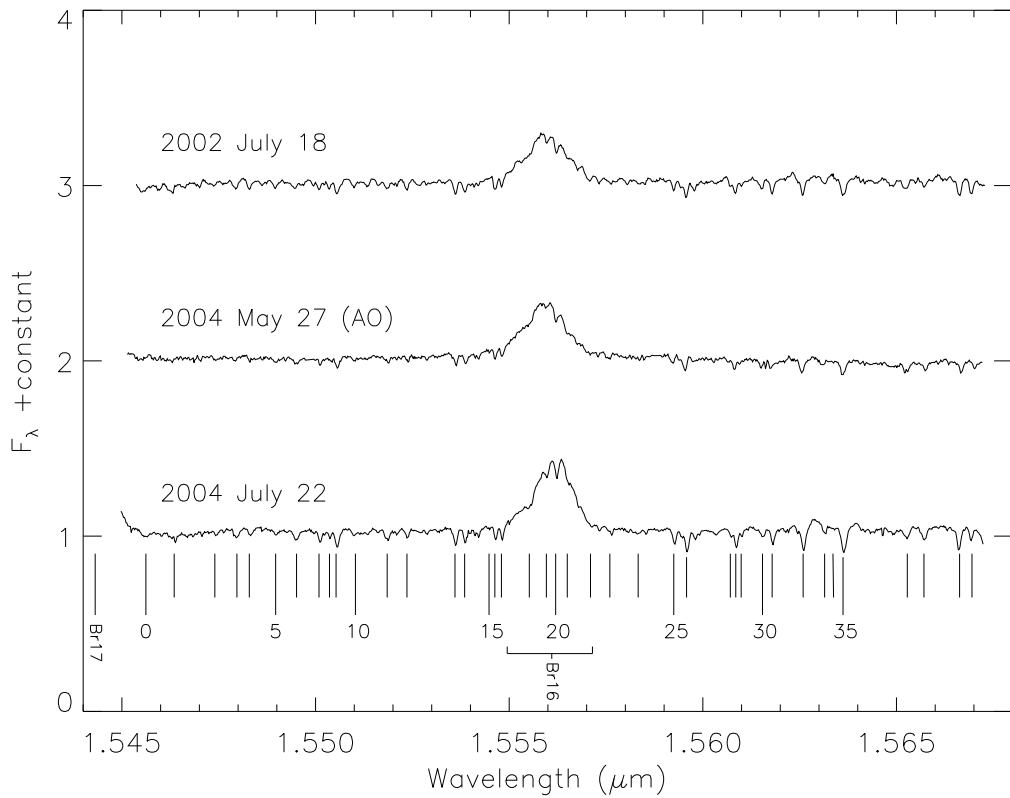


Fig. 2.— Multi-epoch NIRSPEC order 49 spectra of the cTTs AS 353A labeled with UT observation dates. The prominent emission feature is Br16 ($1.5561 \mu\text{m}$). Wavelength and species of identified lines are given in Table 10. All spectra have been wavelength-corrected for heliocentric and radial velocity and normalized to a continuum level of unity.

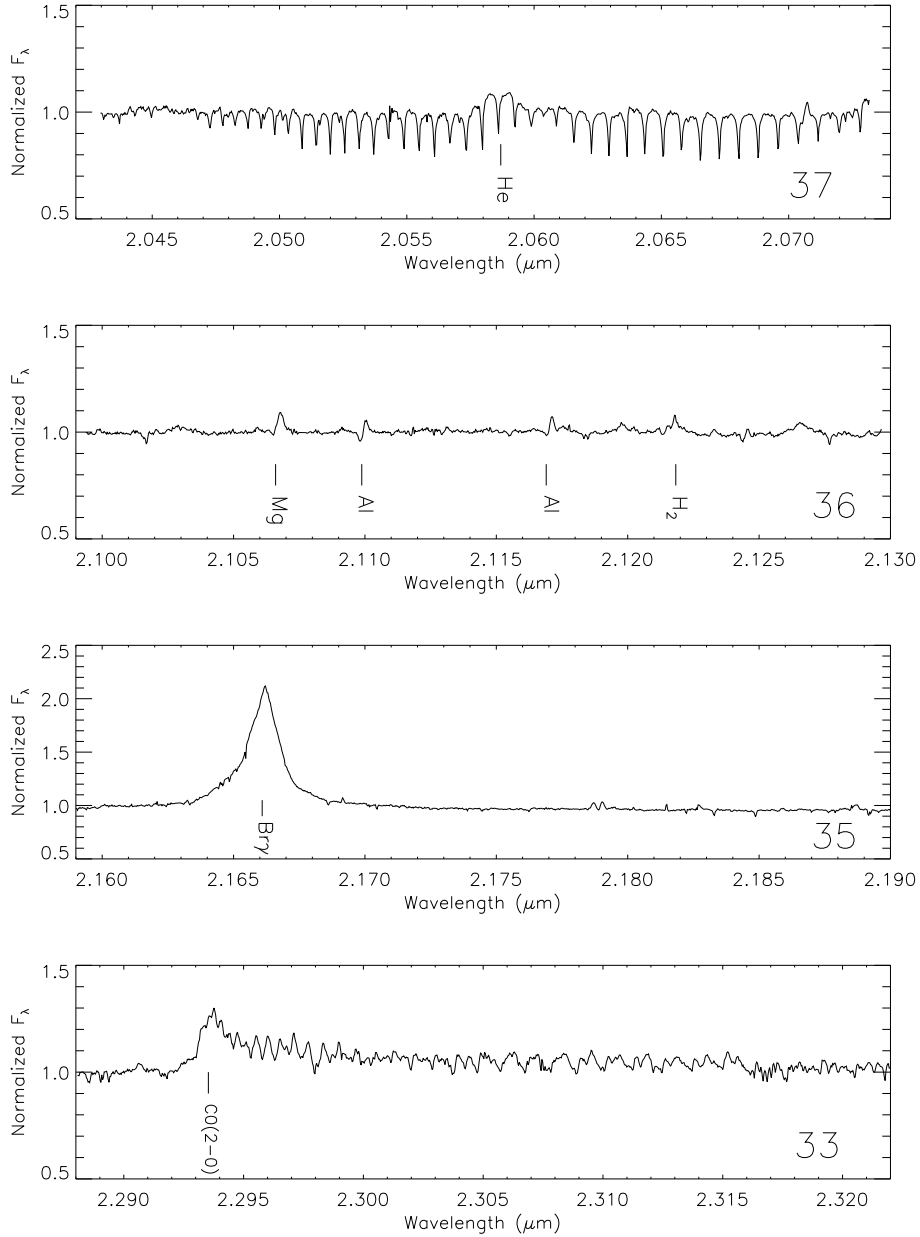


Fig. 3.— Multi-order NIRSPEC K -band spectra of the cTTs AS 353A. All spectra have been normalized to a continuum level of unity within the order and wavelength-corrected for heliocentric and radial velocity. Note that the F_λ range is larger for order 35 in order to show the entire $Br\gamma$ emission line. The series of evenly spaced absorption lines in order 37 is the residue of saturated telluric absorption lines.

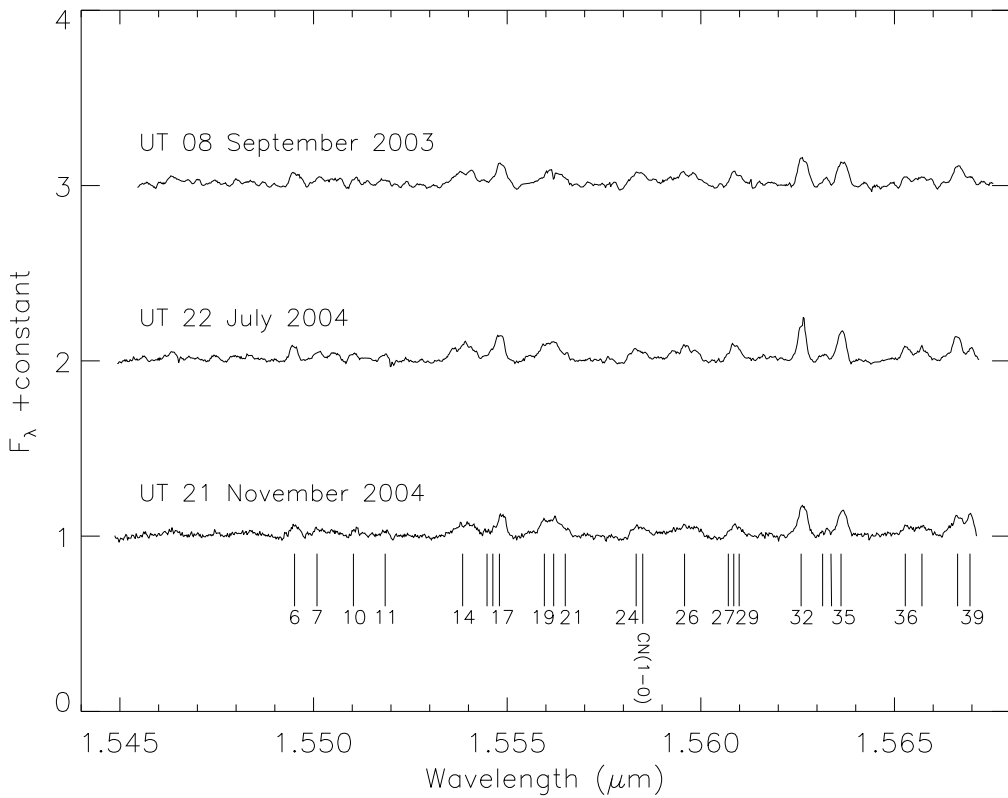


Fig. 4.— Multi-epoch NIRSPEC order 49 spectra of the unusual emission-line object HBC 684. Wavelength and species of identified lines are given in Table 10. All spectra have been wavelength-corrected for heliocentric and radial velocity and normalized to a continuum level of unity.

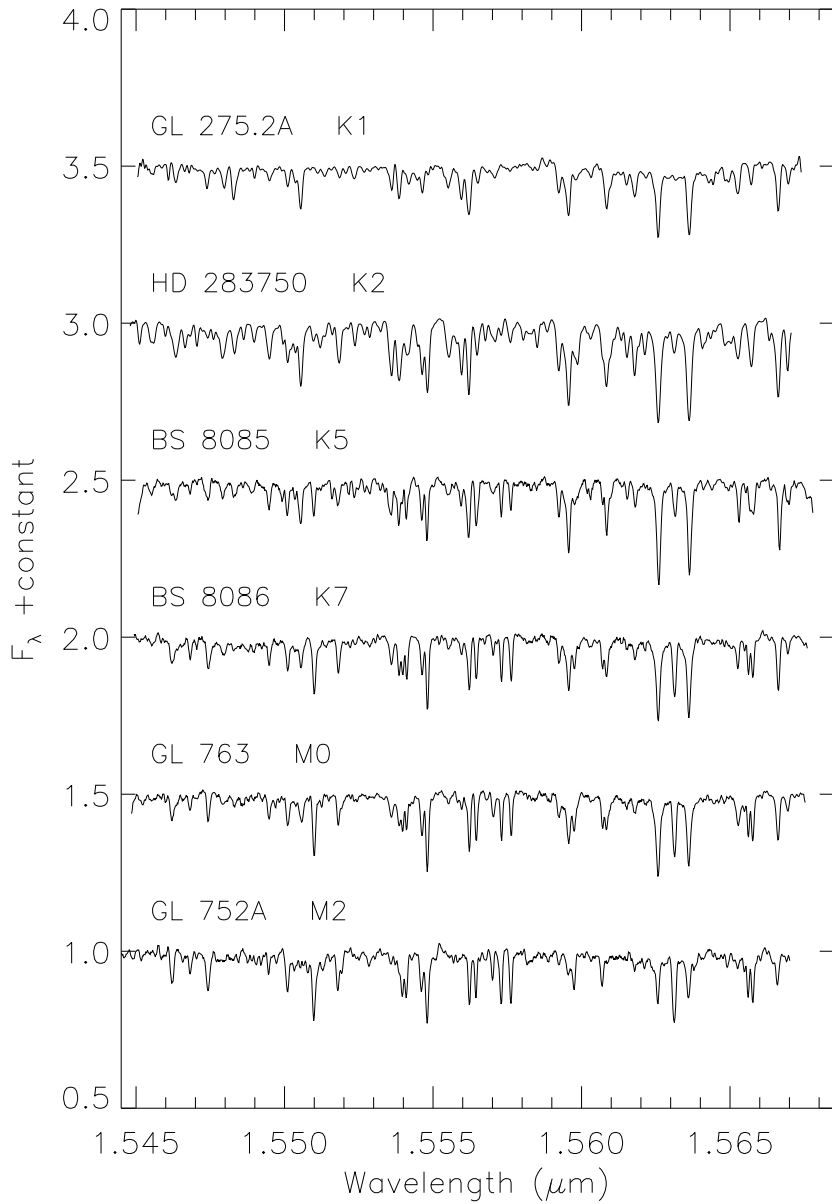


Fig. 5.— Template spectra from Bender et al. (2005) used to determine spectral type and rotational velocity of each sample object. These spectra have been convolved with a $v\sin i=10$ km s $^{-1}$ rotation kernel from Gray (1992). Spectra have also been corrected for heliocentric and radial velocities, normalized to continuum levels of unity, and are presented on the laboratory wavelength scale.

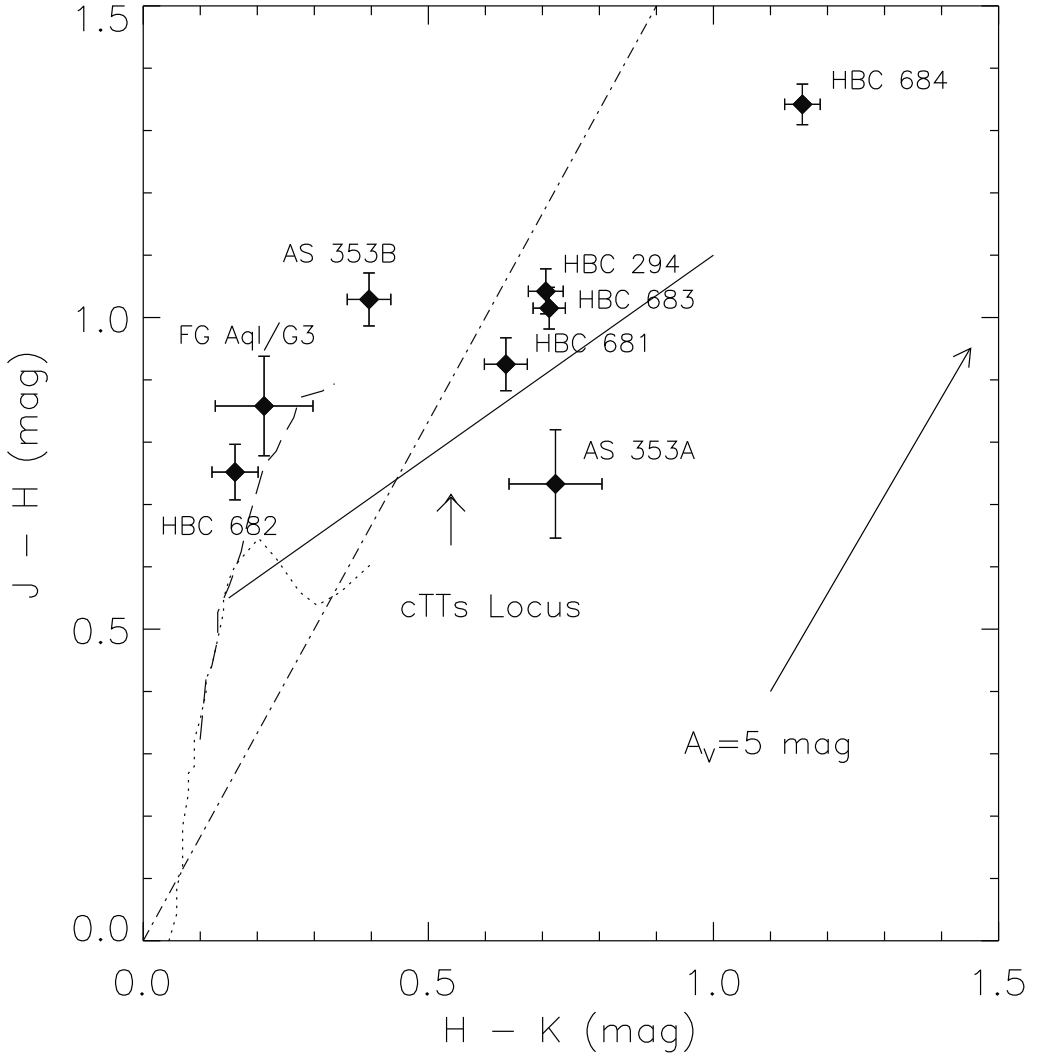


Fig. 6.— $J - H$ versus $H - K$ color-color diagram for the sample objects (Table 8). Magnitudes were taken from 2MASS. Error bars represent the propagated photometric errors reported in the 2MASS catalog. The dash-dotted line separates objects with (to the right) and without IR-excess. The cTTs (solid line), dwarf (dotted line), and giant (dashed line) loci are the same as in Figure 3 of Prato et al. (2003) but transformed in to the 2MASS magnitude scale using equations from Carpenter (2001, §4.3). The effect on observed color of 5 magnitudes of visual extinction is represented by the arrow (thick line), using the equation derived by Prato et al. (2003, §3.1).

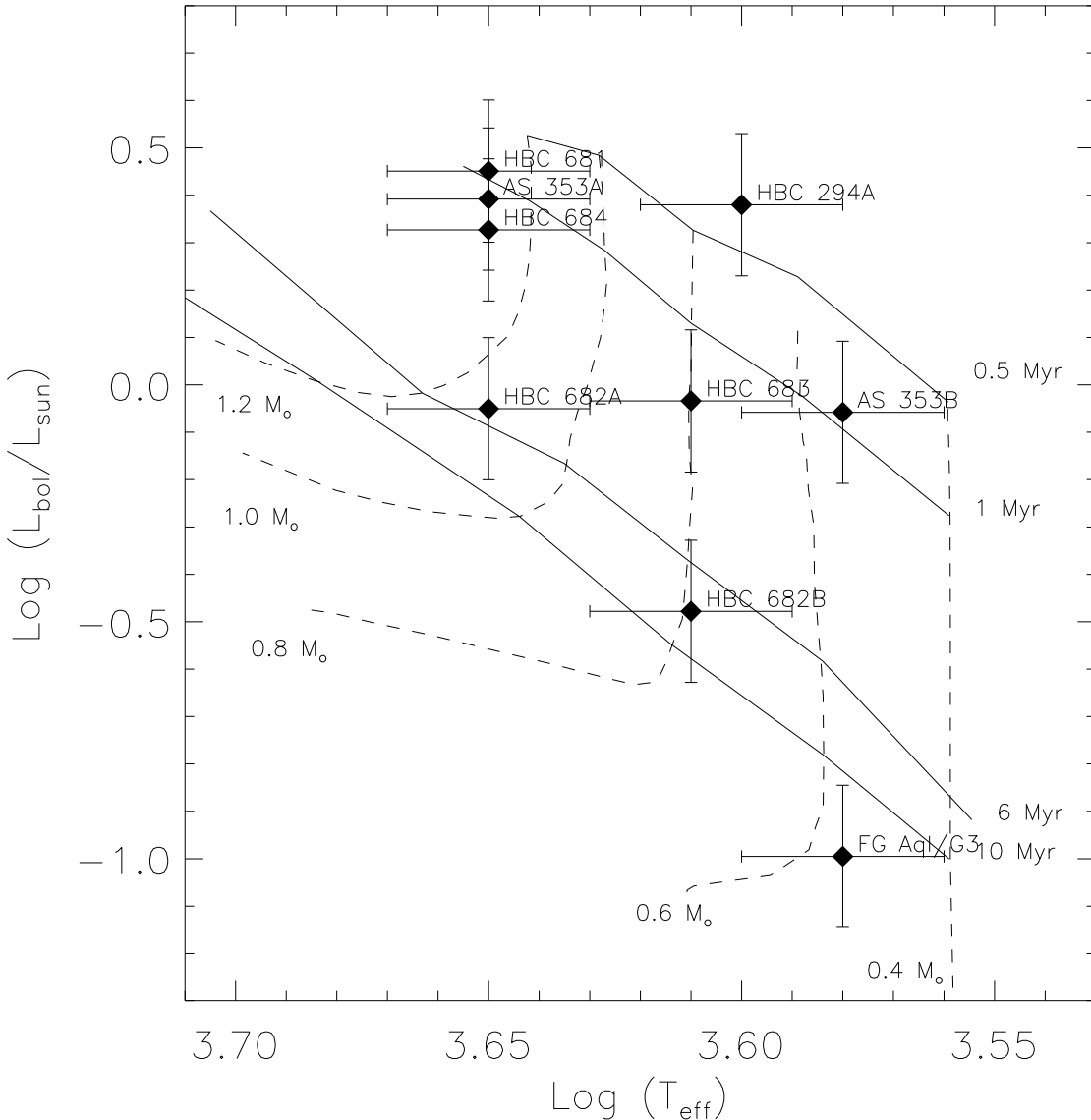


Fig. 7.— H-R diagram of probable Aquila association members using theoretical evolutionary tracks from Palla & Stahler (1999). Mass tracks (dotted lines) are 1.2, 1.0, 0.8, 0.6, and 0.4 solar masses from left to right and isochrones (solid lines) are 5×10^5 , 10^6 , 6×10^6 , and 10^7 years from top to bottom. Temperatures were taken from Luhman (2004) based on the spectral types listed in Table 6. Although AS 353B and HBC 682 were not resolved in 2MASS, their luminosities have been corrected for binarity based on their near-IR flux ratios.